Proceedings for the 6th International Fire Behavior and Fuels Conference
April 29 – May 3, 2019, Sydney, Australia
Published by the International Association of Wildland Fire, Missoula, Montana, USA

Simulated transport of short-range embers in an idealised bushfire

Rahul Wadhwani
Victoria University, Melbourne, Victoria, Australia, rahul.wadhwani@live.vu.edu.au

Duncan Sutherland
University of New South Wales, Canberra, ACT, Australia, duncan.sutherland@adfa.edu.au

Khalid Moinuddin
Victoria University, Melbourne, Victoria, Australia, khalid.moinuddin@vu.edu.au

Introduction

Mega-bushfires like the 2009 Black Saturday, Australia, the 2016 Fort McMurray fire, Canada, and the 2018 Carr fire, USA cause billions of dollars in damage and result in loss of life. The sources of ignition of the fires are often natural or accidental such as lightning, campfire, cigarette butts, or machinery and tools (Miller, Plucinski et al. 2017). The frequency of bushfires is set to increase due to the positive feedback effect of climate change (Jolly, Cochrane et al. 2015). There is an increasing trend of settlement of people at wildland-urban-interface (WUI) (Radeloff, Helmers et al. 2018) which increases the impact of bushfire. Accurate and quick prediction of the evacuation of communities and the behaviour of a bushfire will make a difference in reducing the impact of bushfire (Mell, McDermott et al. 2010, Ronchi, Gwynne et al. 2017).

Operational fire models often have a mean absolute error of 20-80% in estimating the rate of fire spread (Cruz and Alexander 2013). One reason for the large error attributed to the spotting phenomenon. In the spotting phenomenon, burning pieces of debris (commonly called as embers) such as bark, twigs or nuts travel with the wind and land on ignitable vegetative fuel causing new fires called spotfires. Cruz *et al.* (Cruz, Gould et al. 2015) have classified the spotting phenomenon into three categories based on the distance that the embers travel. The three categories are: (a) short-range (500 -750 m), (b) medium-range (1000-1500m), and (c) long-range (>5000 m) spotting. Some operational models include a model for only long-range spotting and many operational models omit spotting entirely (Papadopoulos and Pavlidou 2011, Ronchi, Gwynne et al. 2017).

The McArthur model does include a model of short-range spotting. McArthur (McArthur 1967) observed that in the 1962 Daylesford fire, the original McArthur model significantly underpredicted the rate of fire spread due to the short-range spotting phenomenon. It was observed that due to massive short-range spotting the rate of spread was approximately three times the predicted rate of fire spread if no spotting is assumed. Understanding the short-range spotting with a field experiment is challenging due to the safety of equipment and personnel involved. Moreover, it is difficult to distinguish real embers when they are very close to fire front. Only a handful of studies such as Project Vesta (Gould, McCaw et al. 2008) and Filkov *et al.* (Filkov, Prohanov et al. 2017) have attempted to quantify the behaviour of short-range spotting in eucalyptus and pine forest.

Simulation studies can avoid some of the difficulties associated with field studies. Sardoy *et al.* (Sardoy, Consalvi et al. 2008) developed a short-range spotting model in which embers are generated from a line fire. However, the model was based on an integral plume model rather than the full computational fluid dynamics simulations attempted here. Physics-based fire models (Sullivan 2009) allow full simulation of all fluid transport phenomena from fundamental principles. However, before using any physics-based fire model validation of the inbuilt particle transport model is required (Celik, Ghia et al. 2008). Validation of the physics-based model is challenging as conducting benchmark field scale experiment is difficult due to

the variation of ember properties (Linteris, Gewuerz et al. 2004, Mell, McDermott et al. 2010). However, validation can be conducted using a lab-scale apparatus and scaled up for the field scale which is a standard practice in validation of fire models (Linteris, Gewuerz et al. 2004). We have validated the Lagrangian particle model of Fire Dynamics Simulator (FDS) (McGrattan, McDermott et al. 2015) using an experimental artificial firebrand generator apparatus (Wadhwani, Sutherland et al. 2017).

This work seeks to study the transport of ember particles across realistic forest edges. We seek to compute and characterise the final ember landing distributions, with an eye to developing operational models of ember attack. Such a model will inform scientifically sound forecasts of ember risk from bushfires. Improved forecasts will mitigate the potential risks posed by embers to human lives and properties on the WUI.

We simulate the transport of Lagrangian particles away from a modelled fire within a forest canopy. The particles are tracked across the forest edge and the distributions of embers on the ground were characterised by mean and variances in the x and y directions. Different ember shapes are simulated to understand how ember shape effects the spotting distance and lateral dispersion of embers.

Modelling

The computational domain used in this study is shown in **Error! Reference source not found.**(a). The simulation domain is 1000m long, 160m wide, and 80m high. A uniform rectilinear grid spacing of 2m is used to discretise the domain in X- and Y- direction while vertically (Z- direction) it is discretised at 1m. A logarithmic profile ($u_z = \frac{u_*}{\kappa}\ln(\frac{z-d}{z_0})$) is applied to represent the background wind profile at the inlet of the domain at x=0. The parameters selected are u_*=0.7m/s, d =0 with surface roughness of z_0 =0.3m, and κ=0.4 is von Karman's constant.

The forest canopy is starts at x= 250 which is 250m long, 160m wide and 17m high. It is modelled as a region of aerodynamic drag, where the drag force varies with the leaf area density (LAD) profile [19]. LAD is the measure of the distribution of plant material within the forest canopy. The shear layer of wind immediately above the canopy and the sub-canopy flow are strongly influenced by the LAD. Moon et al. [18] have made detailed LAD measurement for many forests found in Victoria, Australia. LAD is generally heterogeneous in the vertical direction and varies with the type of vegetation. The LAD profile changes as a fire burns the leaf material away. However, for simplicity, we assumed LAD to be constant in time and we also assumed that LAD does not change along the length and breadth of the forest.

We used the LAD profile of the open woodland forest category measured by Moon *et al.* [18]. We fit a Gaussian function (Eq. 1) to the observed LAD data as presented in 1(b). The LAD profile fitted to the data is

$$LAD_{num} = 0.055e^{-(\frac{(z^*-0.85)^2}{0.085})} + 0.02\,, \quad z^* = \frac{z}{H}\,. \qquad \text{Eq. 1}$$

An ember generation plane is defined at 170m inside the canopy which is highlighted with red in **Error! Reference source not found.**. A stationary fire is modelled at the base of the ember generation plane by a region of specified fire intensity at 4714.6 kW/m. The intensity of fire is determined from the data provided for dry sclerophyll eucalyptus by Cruz *et al*. (Cruz, Gould et al. 2015). The ground of the computational domain is assumed to be a rough non-reacting surface. A non-reacting surface assumed to avoid ignition of surface fuel by hot ember particles and to idealise the study to a fixed fire. In reality fires are dynamic which will likely affect the overall ember distribution but is beyond the scope of this initial study.

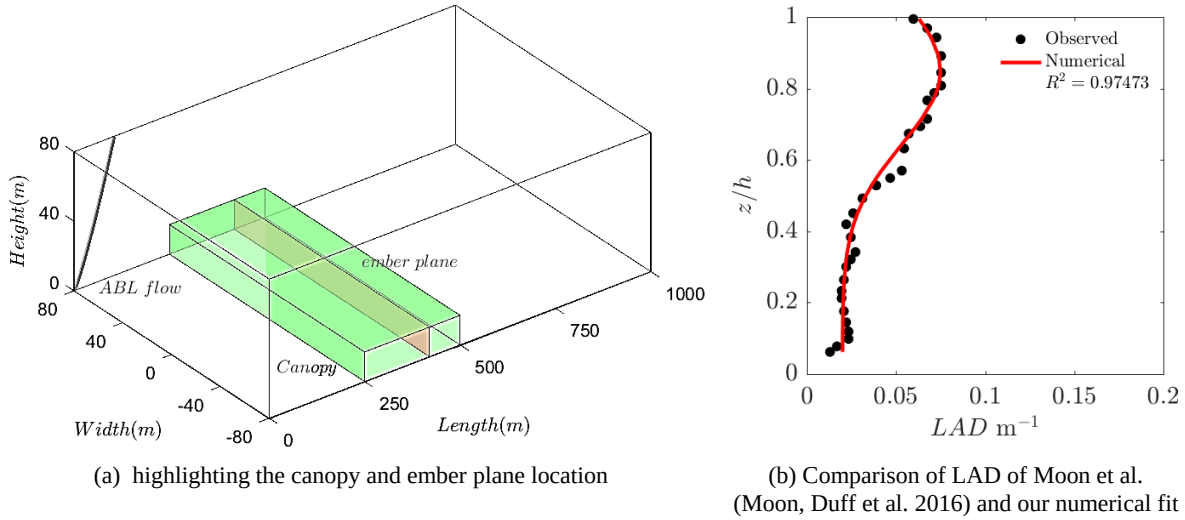

(a) highlighting the canopy and ember plane location

(b) Comparison of LAD of Moon et al. (Moon, Duff et al. 2016) and our numerical fit

Fig, 1 Computational domain with canopy and ember plane location and LAD profile

Periodic boundary conditions are used at the lateral boundaries and constant pressure boundary conditions are used at the outflow and top boundaries. Two shapes of ember particles of density 225kg/m^3 are ejected from the ember plane, (a) square disc and (b) cylindrical shaped embers.

To simulate disc-shaped and cylindrical particles we implemented the Haider and Levenspiel drag models (Haider and Levenspiel 1989) which accounts for the shape of the particle using the sphericity (ψ). The sphericity is the ratio of the surface area of a sphere (which has equivalent volume as of the particle) to the surface area of the particle. The drag model is dependent on particle Reynolds number (Re_D), is given by Eq. 2.

$$C_{D,Ha} = \frac{24}{Re_D}(1 + AR e_D^B) + \frac{C}{1+\frac{D}{Re_D}} \quad , \quad Re_D < 2 \times 10^5 \qquad \text{Eq. 2}$$

Where, $A = exp(2.3288 - 6.4581\psi + 2.4486\psi^2)$,
$B = (0.0964 + 0.5565\psi)$,
$C = exp(4.905 - 13.8944\psi + 18.4222\psi^2 - 10.2599\psi^3)$,
$D = exp(1.4681 + 12.2584\psi - 20.7322\psi^2 + 15.8855\psi^3)$.

The drag model used here is separately validated using an ember generator [17]. The drag model is found to have ~3-5%, ~15-20%, ~10% underprediction in estimating the peak of ember particle distribution for cubiform, cylindrical and square disc particle respectively. This is likely because the rotation of the particles is not accounted for during the simulation.

Three initial particle dimensions for each shape is considered based on the observed ember sizes (Tarifa, del Notario et al. 1965, Manzello and Suzuki 2013, Filkov, Prohanov et al. 2017). The sizes considered for two shapes are: square-disc (Ds1-3) (length and thickness) (10X2.5, 32X2, and 32X4mm) and cylindrical (Cyl1-3) (diameter(Ø) and length) (Ø6X12, Ø6X18, and Ø3X18mm). This yields sphericities of 0.64, 0.338, 0.64, 0.665, 0.832, and 0.779, for Ds1-3 and Cyl1-3 respectively.

The wood material typically ignites around 360-420°C (Li and Drysdale 1992) so initial ember particle temperatures is assumed to be 411°C. The density of the particles is constant throughout the simulations. The ember particles are divided based on its initial height, two regions on the ember plane representing bark (h=0 to 10m) and crown (h=10 to 17m). The simulated wind field is allowed to develop to a statistically steady state for a simulated time of one hour, before particles are injected. After the background flow is steady, four thousand ember particles of each shape and size are injected on the ember plane.

Results

Fig 2 shows the flow contours of temporally averaged centreline streamwise velocity (u-velocity) in the computational domain at the statically steady state. An unperturbed atmospheric surface layer exists before the forest canopy. The forest canopy act as a porous obstruction which reduces the flow speed. At x= 250 m the flow impacts upon the forest canopy. Due to continuity, the flow deflects upwards over the canopy. A shear layer develops above the forest canopy up to x= 420 m where it is disturbed by the plume. Within the canopy, an inflexional profile develops. The velocity is reduced in the leafy crown region but there is a local maximum of velocity in the trunk region near the upstream edge of the canopy.

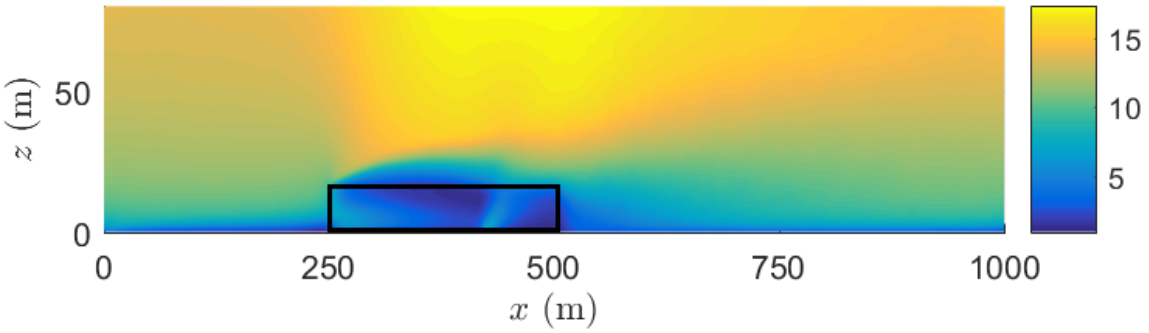

Fig. 2: Mean flow contour in the simulation domain, the canopy is represented with the black line from x=250-500m

The ember distributions for the embers originating in the crown section of the forest canopy are presented in Fig.3. for two example cases: cylindrical Ø6X18 and square-disc-32X2. The lateral dispersion of ember particles is computed as the signed difference between the final and initial y-locations of the particle, so the mean distance in the y-direction (lateral dispersion) is zero. The bivariate probability distribution function (pdf) of cylindrical embers is estimated from the histogram of final ember location normalised so that the volume under the surface is one. The pdf of embers shows only the first impact location on the ground; bouncing of ember particles is not considered.

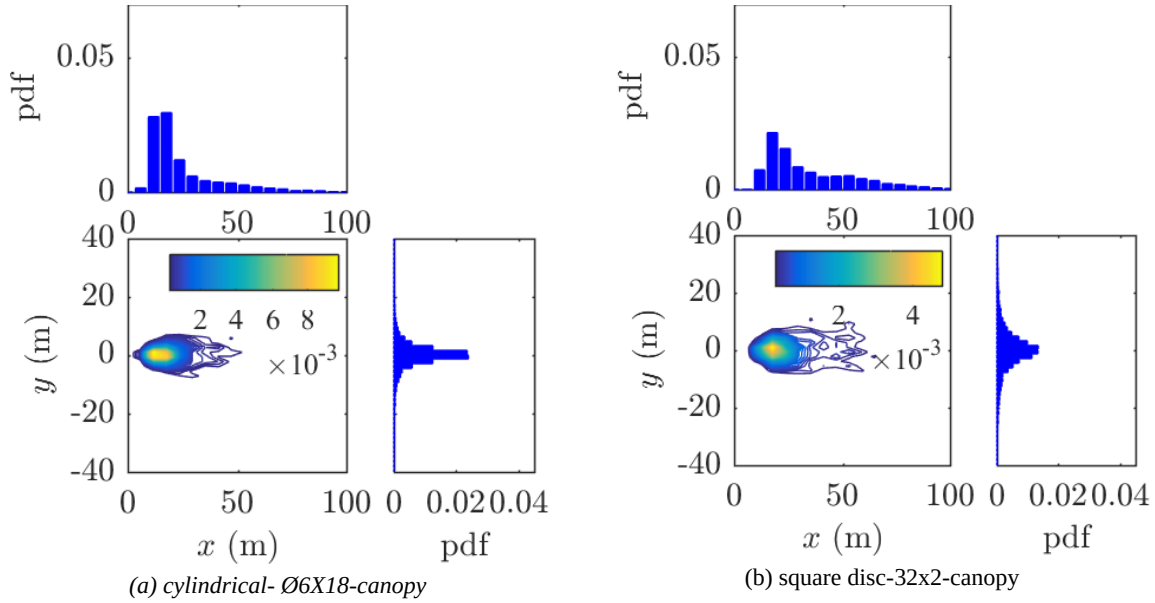

(a) cylindrical- Ø6X18-canopy

(b) square disc-32x2-canopy

Fig. 3: Spatial distribution for cylindrical particle and square disc ember particles at initial temperature of 411°C

The marginal pdfs in the x- and y-directions are computed by summing the bivariate pdf in the y- and x-directions respectively. The contours of the bivariate pdf, the x- and y-marginal distributions of cylindrical embers are shown in Fig. 3a. The same distributions for the square

disc particles-32x2mm are shown in Fig. 3b. The observations show that cylindrical ember particles are more concentrated compared to square disc ember particles, which can be seen from the colour scale used in Fig 3. The distributions of embers in x-direction are observed to be qualitatively similar with the field study in Project Vesta for short-range embers (Gould, McCaw et al. 2008). Fig. 4 (a) and (b) are box-and-whisker plots of the x- and y-distances that the particle travels. The box-and-whisker plots shows the variation in the distributions of all six type of embers generated from crown and trunk section on the firebrand plane. The maximum spotting distance of ember in our study is defined as the maximum distance up to which 95% of the ember falls which are shown by black dots in Fig 4.

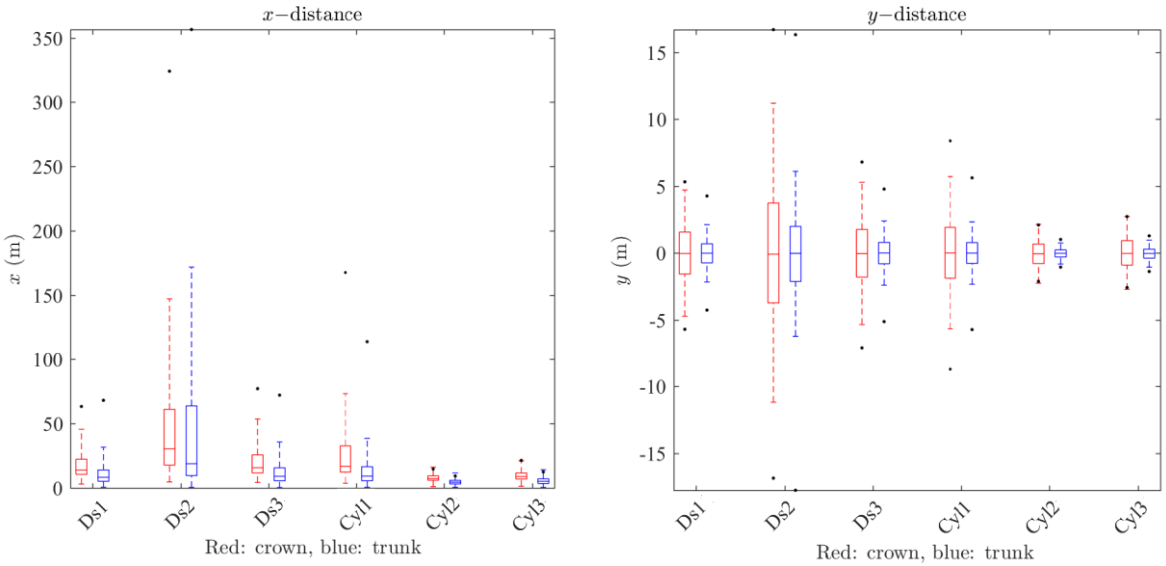

(a) x-distance

(b) y-distance

Fig. 4: Variation of median, first and third quartiles in streamwise (x-direction) and crosswise direction (y-direction). Black dots denote the maximum distance up to which 95% ember falls

Square disc embers found to generally travel farther compared with cylindrical embers and the square disc ember particles are observed to disperse more compared to cylindrical embers in crosswise (y-) direction. The dispersal of the embers will depend on both the mass (given by the volume of the particle, because the density of the particle is constant) and the sphericity of the particle. The square disc particles have significantly smaller sphericity compared to the cylindrical particles and consequently the square disc particles are more dispersed than the cylindrical particles. The initial height of the ember appears significant to the final ember distribution. In almost all cases, the embers released from the trunk area travel a shorter distance than the embers released from the crown.

Conclusions

Prior to this work, there were no known computational studies of transport of short-range embers in a forest canopy. We have demonstrated that physics-based simulations can be used to study short-range embers transported away from a fire. The x-distance results are qualitatively similar to the observations made in Project Vesta (Gould, McCaw et al. 2008). The shape of the ember particle critically affects the maximum spotting distance and the dispersion of the particles. Future work will investigate the effect of the canopy type on ember transport and lead to operational models for short-range ember transport.

References:

Celik, I. B., U. Ghia and P. J. Roache (2008). "Procedure for estimation and reporting of uncertainty due to discretization in CFD applications." Journal of Fluids Engineering **130**(7).

Cruz, M. G. and M. E. Alexander (2013). "Uncertainty associated with model predictions of surface and crown fire rates of spread." Environmental Modelling & Software **47**: 16-28.
Cruz, M. G., J. S. Gould, M. E. Alexander, A. L. Sullivan, W. L. McCaw and S. Mathews (2015). Guide to Rate of Fire Spread Models for Australian Vegetation, CSIRO Land and Water Flagship, Canberra, ACT and AFAC, Melbourne, VIC.
Filkov, A., S. Prohanov, E. Mueller, D. Kasymov, P. Martynov, M. El Houssami, J. Thomas, N. Skowronski, B. Butler and M. Gallagher (2017). "Investigation of firebrand production during prescribed fires conducted in a pine forest." Proceedings of the Combustion Institute **36**(2): 3263-3270.
Gould, J. S., W. McCaw, N. Cheney, P. Ellis, I. Knight and A. Sullivan (2008). Project Vesta: fire in dry eucalypt forest: fuel structure, fuel dynamics and fire behaviour, Csiro Publishing.
Haider, A. and O. Levenspiel (1989). "Drag coefficient and terminal velocity of spherical and nonspherical particles." Powder technology **58**(1): 63-70.
Jolly, W. M., M. A. Cochrane, P. H. Freeborn, Z. A. Holden, T. J. Brown, G. J. Williamson and D. M. Bowman (2015). "Climate-induced variations in global wildfire danger from 1979 to 2013." Nature communications **6**: 7537.
Li, Y. and D. Drysdale (1992). "Measurement of the ignition temperature of wood." Fire Safety Science **1**: 380-385.
Linteris, G. T., L. Gewuerz, K. B. McGrattan and G. P. Forney (2004). "Modeling solid sample burning with FDS." National Institute of Standards and Technology, NISTIR **7178**: 36.
Manzello, S. L. and S. Suzuki (2013). "Experimentally simulating wind driven firebrand showers in Wildland-Urban Interface (WUI) fires: overview of the NIST firebrand generator (NIST dragon) technology." Procedia Engineering **62**: 91-102.
McArthur, A. G. (1967). "Fire behaviour in eucalypt forests."
McGrattan, K., R. McDermott, C. Weinschenk, K. Overholt, S. Hostikka and J. Floyd (2015). Fire dynamics simulator (Sixth Edition) user's guide. Special publication 1019. Gaithersburg, Maryland, USA, National Institute of Standards and Technology**:** 280.
Mell, W. E., R. J. McDermott and G. P. Forney (2010). Wildland fire behavior modeling: perspectives, new approaches and applications. Proceedings of 3rd Fire Behavior and Fuels Conference,, Spokane, Washington, USA.
Miller, C., M. Plucinski, A. Sullivan, A. Stephenson, C. Huston, K. Charman, M. Prakash and S. Dunstall (2017). "Electrically caused wildfires in Victoria, Australia are over-represented when fire danger is elevated." Landscape and Urban Planning **167**: 267-274.
Moon, K., T. Duff and K. Tolhurst (2016). "Sub-canopy forest winds: understanding wind profiles for fire behaviour simulation." Fire Safety Journal.
Papadopoulos, G. D. and F.-N. Pavlidou (2011). "A comparative review on wildfire simulators." IEEE systems Journal **5**(2): 233-243.
Radeloff, V. C., D. P. Helmers, H. A. Kramer, M. H. Mockrin, P. M. Alexandre, A. Bar-Massada, V. Butsic, T. J. Hawbaker, S. Martinuzzi and A. D. Syphard (2018). "Rapid growth of the US wildland-urban interface raises wildfire risk." Proceedings of the National Academy of Sciences **115**(13): 3314-3319.
Ronchi, E., S. Gwynne, G. Rein, R. Wadhwani, P. Intini and A. Bergstedt (2017). e-Sanctuary: Open Multi-Physics Framework for Modelling Wildfire Urban Evacuation. Quincy, MA, USA, , Fire Protection Research Foundation.
Sardoy, N., J. Consalvi, A. Kaiss, A. Fernandez-Pello and B. Porterie (2008). "Numerical study of ground-level distribution of firebrands generated by line fires." Combustion and Flame **154**(3): 478-488.
Sullivan, A. L. (2009). "Wildland surface fire spread modelling, 1990–2007. 1: Physical and quasi-physical models." International Journal of Wildland Fire **18**(4): 349-368.
Tarifa, C. S., P. P. del Notario and F. G. Moreno (1965). On the flight paths and lifetimes of burning particles of wood. Symposium (International) on Combustion, Elsevier.
Wadhwani, R., D. Sutherland, A. Ooi, K. Moinuddin and G. Thorpe (2017). "Verification of a Lagrangian particle model for short-range firebrand transport." Fire Safety Journal **91**: 776-783.